Article

Frequency ratio of the ^{229m}Th nuclear isomeric transition and the ^{87}Sr atomic clock

https://doi.org/10.1038/s41586-024-07839-6

Received: 20 June 2024

Accepted: 17 July 2024

Published online: 4 September 2024

Check for updates

Chuankun Zhang[1,2,3]✉, Tian Ooi[1,2,3], Jacob S. Higgins[1,2,3], Jack F. Doyle[1,2,3], Lars von der Wense[1,2,3,7], Kjeld Beeks[4,8], Adrian Leitner[4], Georgy A. Kazakov[4], Peng Li[5], Peter G. Thirolf[6], Thorsten Schumm[4] & Jun Ye[1,2,3]✉

Optical atomic clocks[1,2] use electronic energy levels to precisely keep track of time. A clock based on nuclear energy levels promises a next-generation platform for precision metrology and fundamental physics studies. Thorium-229 nuclei exhibit a uniquely low-energy nuclear transition within reach of state-of-the-art vacuum ultraviolet (VUV) laser light sources and have, therefore, been proposed for construction of a nuclear clock[3,4]. However, quantum-state-resolved spectroscopy of the ^{229m}Th isomer to determine the underlying nuclear structure and establish a direct frequency connection with existing atomic clocks has yet to be performed. Here, we use a VUV frequency comb to directly excite the narrow ^{229}Th nuclear clock transition in a solid-state CaF_2 host material and determine the absolute transition frequency. We stabilize the fundamental frequency comb to the JILA ^{87}Sr clock[2] and coherently upconvert the fundamental to its seventh harmonic in the VUV range by using a femtosecond enhancement cavity. This VUV comb establishes a frequency link between nuclear and electronic energy levels and allows us to directly measure the frequency ratio of the ^{229}Th nuclear clock transition and the ^{87}Sr atomic clock. We also precisely measure the nuclear quadrupole splittings and extract intrinsic properties of the isomer. These results mark the start of nuclear-based solid-state optical clocks and demonstrate the first comparison, to our knowledge, of nuclear and atomic clocks for fundamental physics studies. This work represents a confluence of precision metrology, ultrafast strong-field physics, nuclear physics and fundamental physics.

Time and frequency are the most precisely measured physical quantities in experimental physics[1,5]. Using ultranarrow linewidth electronic transitions in the visible spectral domain, current optical atomic clocks have achieved measurement precision better than 1×10^{-20} and systematic uncertainty at 8×10^{-19} in fractional frequency units[2]. These systems are poised to explore fundamental physics such as measurements of quantum effects under gravity and searches for new physics beyond the standard model[6].

The tremendous progress of optical atomic clocks traces its scientific roots to increasingly higher quality factors of natural resonances, highly coherent lasers, precise quantum-state control of relevant atomic degrees of freedom, understanding of complex many-body physics and strong connections to fundamental physics. These important ingredients form the foundation of the next generation of clocks. Harnessing natural resonances in the vacuum ultraviolet (VUV) spectrum and beyond while maintaining long coherence times naturally leads to higher quality factors. A clock based on a fundamentally new platform could greatly advance the ability of tabletop experiments to explore new physics. Another increasingly important need is to take clocks out of the laboratory without adversely impacting their precision or accuracy.

It is with this scientific context that a low-lying thorium-229 nuclear transition has emerged as a highly desirable candidate for the next-generation clock[3,4]. Notably, the metastable isomeric state ^{229m}Th is only 8.4 eV (approximately 148 nm) higher in energy than the ground state, with a lifetime[7–9] of approximately 10^3 s. This nuclear transition is lower in frequency than almost every other known nuclear transition by several orders of magnitude owing to a nearly exact cancellation of the megaelectronvolt level nuclear energy terms. Therefore, precise laser spectroscopy of the ^{229}Th nuclear transition dramatically enhances the sensitivity of tests of fundamental physics[8,10,11], such as searches for ultralight dark-matter candidates, or temporal variations of the fine-structure constant and the dimensionless strong-interaction parameter. It has also been proposed for the study of fundamental electron–nuclear coupling interactions, such as the electron-bridge process[12]. Furthermore, the nuclear transition is highly insensitive to external electromagnetic perturbations[3], making it an ideal portable clock.

Over the past two decades, the determination of the energy and properties of ^{229m}Th has steadily advanced, initially indirectly[13–16] and most recently from a flurry of nuclear physics experiments[17–21] after the first detection of the internal conversion decay[22] of ^{229m}Th. The first

[1]JILA, University of Colorado Boulder, Boulder, CO, USA. [2]NIST, Boulder, CO, USA. [3]Department of Physics, University of Colorado Boulder, Boulder, CO, USA. [4]Vienna Center for Quantum Science and Technology, Atominstitut, TU Wien, Vienna, Austria. [5]IMRA America, Ann Arbor, MI, USA. [6]Ludwig-Maximilians-Universität München, Garching, Germany. [7]Present address: Johannes Gutenberg-Universität Mainz, Institut für Physik, Mainz, Germany. [8]Present address: Laboratory for Ultrafast Microscopy and Electron Scattering (LUMES), Institute of Physics, École Polytechnique Fédérale de Lausanne (EPFL), Lausanne, Switzerland. ✉e-mail: chuankun.zhang@colorado.edu; ye@jila.colorado.edu

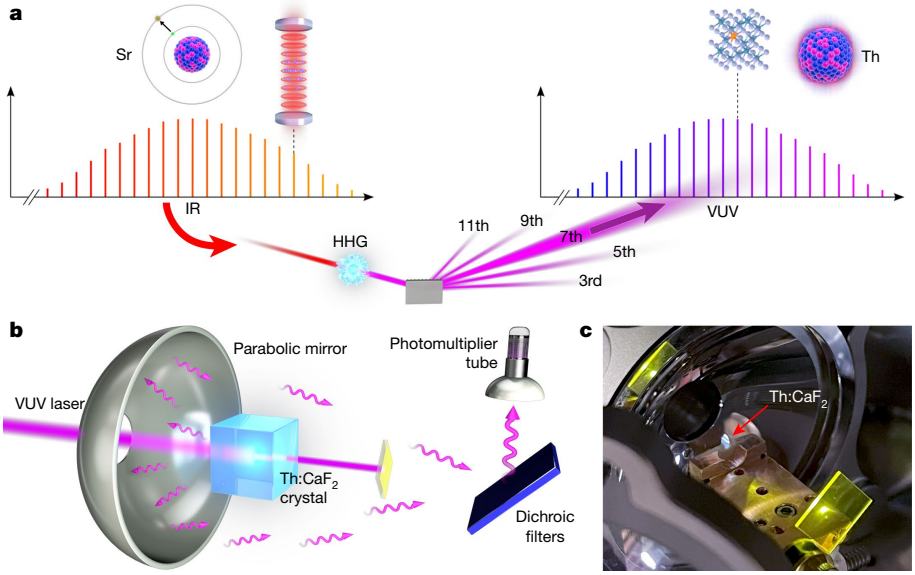

Fig. 1 | VUV comb spectroscopy of the ^{229}Th nuclear clock transition. a, An infrared frequency comb with a 75 MHz repetition frequency is stabilized by the JILA ^{87}Sr optical lattice clock[2]. The infrared frequency comb is upconverted to VUV through a coherent, high-order harmonic generation (HHG) process inside a femtosecond enhancement cavity (not shown). A single VUV comb line in the seventh harmonic comb (approximately 148.3 nm centre wavelength) directly excites the ^{229}Th nuclear clock transition, providing a direct frequency connection between the nuclear and atomic clocks. A representative crystal structure[53] of ^{229}Th:CaF_2 is shown with the doped ^{229}Th coloured orange. **b**, Illustration of the detection setup. After 400 s illumination, the excitation comb is shut off. Fluorescent photons from the decay of ^{229m}Th embedded in the CaF_2 crystal are collected by using a VUV-reflective parabolic mirror. A series of dichroic filters (only one shown) steer photons at the nuclear transition wavelength to a detector while suppressing background photons. A PMT is used to count individual VUV fluorescent photons for 200 s while the comb is off. **c**, Photograph of the Th:CaF_2 crystal under VUV irradiation. The Th:CaF_2 crystal scintillates, showing a visible white–blue trace of the laser path. A fluorescent screen (yellow) blocks the VUV comb transmission through the Th:CaF_2 crystal to protect the PMT from laser damage. The yellow fluorescence signal is also used for laser alignment and power monitoring.

direct observation of the radiative decay[23] of ^{229m}Th was reported from CERN only a year ago, by using ^{229}Ac implanted into a CaF_2 crystal. After beta decay, a large fraction of the daughter isotopes branched into the ^{229m}Th state, and their subsequent radiative decay photons were detected on a VUV spectrometer. This measurement placed the transition frequency uncertainty at the terahertz level and reported a radiative decay half-life of 670(102) s, corresponding to a lifetime of 967(147) s (here and throughout, the numbers in parentheses represent the 1 − σ uncertainty). Later, a group from Okayama University used X-rays to pump a Th-doped CaF_2 crystal to the second excited state[24] of 29 keV, which partially decayed to ^{229m}Th and yielded a radiative decay with a half-life of 447(25) s (lifetime 645(36) s). Another recent experiment at RIKEN successfully trapped isomeric $^{229m}Th^{3+}$ (populated via ^{233}U decay) in an ion trap[25] and measured a half-life of $1{,}400^{+600}_{-300}$ s (lifetime $2{,}020^{+866}_{-433}$ s).

The first resonant excitation was reported at Physikalisch-Technische Bundesanstalt (PTB) by using a ^{229}Th-doped CaF_2 crystal irradiated by a nanosecond pulsed VUV laser generated via four-wave mixing[26]. This result was soon independently verified in a ^{229}Th-doped $LiSrAlF_6$ crystal at the University of California, Los Angeles, through the use of a similar four-wave mixing light source[27]. These two measurements observed a single resonance profile with a laser-limited linewidth on the order of 10 GHz and placed the uncertainty of the transition at a similar frequency scale. The fluorescent lifetimes reported in the CaF_2 and $LiSrAlF_6$ crystals were 630(15) s and $568(13)_{stat}(20)_{sys}$ s, respectively. The different isomer lifetimes observed in these experiments can be attributed to the Purcell effect, where a higher refractive index of the crystalline environment leads to a higher density of photon states[28].

In this work, we follow the early proposals[29,30] and embed ^{229}Th in a solid-state CaF_2 crystal. We probe the narrow nuclear clock transition directly with a single line of a VUV frequency comb. The VUV comb is generated via a coherent high-harmonic-generation process and is frequency stabilized to the JILA ^{87}Sr optical clock[2]. In the demonstrated precision spectroscopy of the ^{229}Th nuclear clock transition, we directly resolve the narrow line structure arising from the interaction between the nuclear electric quadrupole moments and the crystal electric field gradient. We determine the absolute transition frequency to the kilohertz level. This work establishes a milestone for direct frequency connection between a nuclear clock and an optical atomic clock, provides an enhanced determination of important parameters of the nucleus and the crystal field and paves the way to search for temporal variations of fundamental constants and the development of a portable nuclear clock based on ^{229}Th-doped crystals.

Direct frequency link between the ^{87}Sr atomic clock and the ^{229m}Th isomeric transition

The JILA Sr lattice clock[2] serves as the absolute frequency reference for our fundamental comb in the infrared (Fig. 1a). A local oscillator at 698 nm, which serves as the Sr clock laser, is stabilized to a cryogenic silicon cavity[31] operated at 1.5 μm via a separate optical frequency comb, inheriting excellent frequency stability. The absolute frequency of the Sr clock laser is periodically calibrated with the JILA Sr lattice clock[2] to correct for long-term drifts. Although we did not actively perform a systematic evaluation of the Sr clock, its overall uncertainty is estimated to be below 1×10^{-16} across the period of our measurements[32], providing a sufficiently accurate frequency reference for the ^{229}Th transition frequency determination.

Frequency combs are ideal tools to transfer optical frequency references across large wavelength ranges[33]. Their strictly equidistant comb lines permit the precise and direct readout of optical frequencies, and their femtosecond pulsed nature in the time domain allows efficient nonlinear frequency conversion[34] to different spectral domains. To connect the absolute frequency of the ^{87}Sr clock laser to the ^{229}Th nuclear transition frequency, we use a VUV comb-generation process.

Frequency combs in the vacuum-to-extreme ultraviolet have been under continuous development over the past two decades[35–39]. Our specific VUV frequency comb apparatus is described in a previous publication[40]. We start with a Yb-fibre oscillator[41], followed by nonlinear preamplification and chirped pulse power amplification with a large mode area Yb-doped fibre to reach an average output power of 40–50 W. We use a femtosecond enhancement cavity for coherent enhancement of the infrared comb, obtaining an intracavity train of femtosecond pulses with an average power of approximately 5–7 kW and pulse durations of approximately 150–200 fs. The intracavity infrared pulse is focused (peak intensity approximately 10^{13} W cm^{-2}) into a xenon gas jet for efficient seventh harmonic generation. To ensure our seventh harmonic centres around 148.3 nm, we bandpass filter the seed spectrum before the final Yb-fibre amplifier to a centre wavelength of 1,038 nm. The VUV comb spectral envelope width is approximately 1 nm, fully covering the known uncertainty range of the nuclear transition. A high repetition rate of 75 MHz is chosen to preserve the optical phase coherence and generate well-separated comb lines for precision spectroscopy.

To prepare for high-resolution spectroscopy and clock operation on the nuclear transition, we have made several critical improvements to our VUV frequency comb apparatus. We use a grazing incidence plate[42,43] to outcouple the VUV comb with approximately 50% efficiency. We translate the plate to a new spot approximately every 10 h to avoid VUV-induced plate degradation. A home-built xenon recycling system is installed to reduce the operational cost from using a continuous gas jet. By engineering for excellent passive thermal stability, we achieve stable, continuous, full-power operation of the VUV comb for many days, during which only occasional relocking and maintenance of the laser is needed.

The outcoupled seventh harmonic is selectively reflected to the ^{229}Th target by using a multilayer coated mirror. In addition, we take advantage of the chromatic dispersion in a MgF_2 lens to further filter out other harmonics geometrically. We estimate the available power in the seventh harmonic on the target to be approximately 200 μW, corresponding to 1 nW per comb mode.

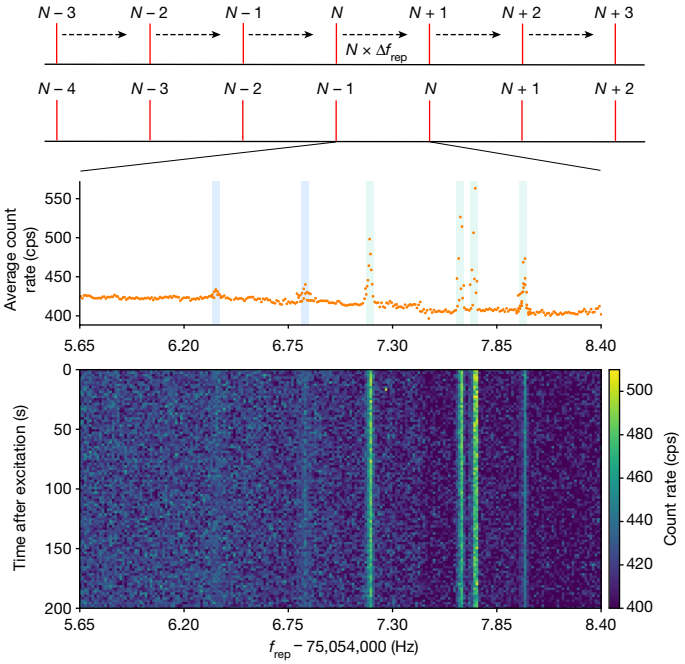

Fig. 2 | A full-range comb scan. The VUV comb repetition rate is scanned by precisely tuning f_{rep} to shift all the comb lines in parallel. The optical frequency gap between adjacent comb lines is fully covered when the Nth comb mode overtakes the original frequency position of the $(N+1)$ comb mode (top panel). Experimentally, the precise f_{rep} control is achieved by fixing f_{CEO}, then digitally changing the phase lock offset frequency between the ^{87}Sr clock laser and its nearest comb line. The average fluorescence photon count rate per second (cps) in the 200 s detection window is plotted against the comb repetition rate. Six distinct spectroscopic features are observed and highlighted in blue and green (middle panel). Four dominant peaks (green), which we later assign to electric quadrupole splittings of the nuclear transition, will be used for absolute frequency determination. The count rate as a function of time (colour bar; units in cps) at each frequency bin is plotted in the bottom panel, highlighting a nuclear excited-state lifetime that is significantly longer than the detection window.

Spectroscopy setup

A ^{229}Th:CaF_2 single crystal with a doping concentration of 5×10^{18} cm^{-3} was grown at TU Wien by using a miniaturized vertical gradient freeze method followed by a fluorination treatment[44,45]. A small piece ($1.8 \times 0.7 \times 1.4$ mm^3) of this ^{229}Th:CaF_2 crystal was cut and polished for this experiment. Fluorescence from the ^{229m}Th isomer has been observed in crystals cut from the same ingot at both PTB[26] and Okayama University[24].

The crystal is mounted at the focus of a parabolic collection mirror and cooled down to 150(1) K (Methods). We illuminate the crystal with our VUV beam (0.2 mm diameter) along the 1.4 mm length direction. Fluorescence photons collimated by the parabolic mirror are selectively steered with a series of multilayer coated filters (150±10 nm) to a photomultiplier tube (PMT) for single photon counting. Figure 1b shows a conceptual visualization and Fig. 1c a photo of the setup. The CaF_2 crystal scintillates, tracing out our VUV beam path as the thin line shown in the photo. The transmitted laser is terminated at the yellow Ce:YAG fluorescent plate. The effective efficiency of the setup, from the nucleus emitting a photon to a count collected on the PMT, is estimated to be 0.3%.

Comb locking and full-range scan

For comb stabilization, a supercontinuum of the infrared comb is generated in a highly nonlinear fibre with a picked off portion of the preamplified light. The supercontinuum light is used in the f–$2f$ referencing scheme to stabilize the carrier-envelope offset frequency f_{CEO} to a radiofrequency reference. The f_{CEO} lock point is chosen to be −8 MHz to match the dispersion in the femtosecond enhancement cavity[35,36]. We phase lock one of the supercontinuum comb lines to the ^{87}Sr clock laser with an offset frequency f_{beat} set by a direct digital synthesizer. Changing f_{beat} while fixing f_{CEO} allows us to precisely tune the comb repetition rate f_{rep}. In addition, a narrow linewidth Mephisto laser at 1,064 nm is used as a short-term reference to stabilize the comb linewidth, the frequency of which is slowly steered to maintain the phase lock between the supercontinuum comb and the Sr clock laser. The Mephisto laser also serves as an auxiliary laser for stabilizing the enhancement cavity length (Methods).

The seventh harmonic has a frequency comb structure with the same repetition rate as the fundamental, but an offset frequency of $7 \times f_{CEO}$ and integer comb mode numbers $N \approx 2.7 \times 10^7$. To search for the transition, we scan f_{rep} in the range of approximately 2.8 Hz to scan the comb structure underneath the seventh harmonic spectral envelope without changing the envelope itself. This scan range is multiplied by the large comb mode number N in the VUV domain, making the frequency of the Nth comb mode at the end of scan overlap the starting point for the $(N+1)$ comb mode frequency (Fig. 2, top panel). Thus, we fully cover the spectrum under the approximately 1 nm wide comb spectral envelope.

A typical experimental cycle consists of two parts: irradiation and photon detection. We start by irradiating the crystal for 400 s, during which the PMT is turned off to avoid damage from scattered VUV photons.

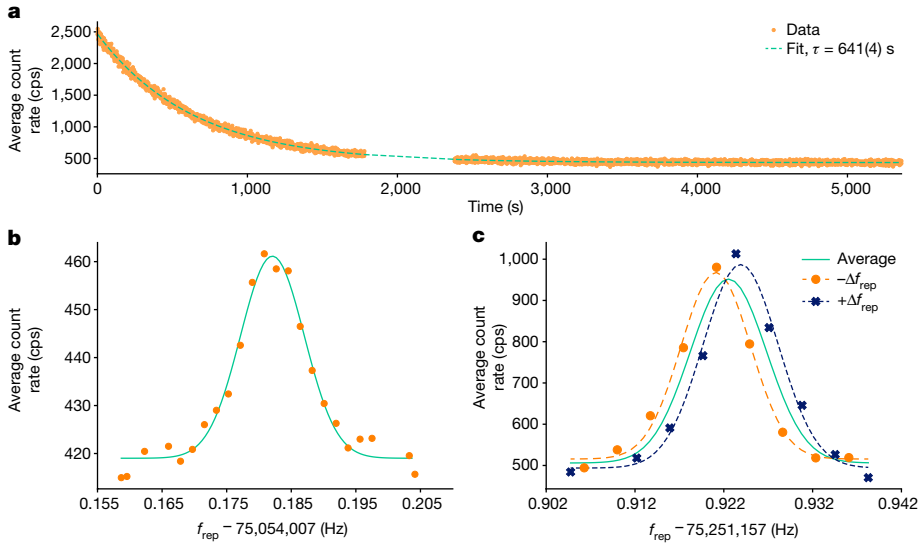

Fig. 3 | Line shape and centre frequency determination. a, Lifetime measurement of the excited clock state ^{229m}Th ($m_g = \pm 5/2$ to $m_{is} = \pm 3/2$ transition, Fig. 5, line b). The fluorescence photon count rate is monitored over time after laser excitation of 1,200 s. A portion of the data around 2,000 s is absent owing to technical reasons. The experimental data is fit with a single exponential decay, leaving no structure in the fit residual. The extracted lifetime of the nuclear excited state is 641(4) s in the CaF_2 host crystal. **b**, Fine scan showing the line shape (Fig. 5, line a) for one of the main clock transitions. We wait 1,800 s in between each data point to avoid line-shape asymmetry that could arise from residual excited population from previous scan steps. The fitted Gaussian full-width at half-maximum is 0.0116(5) Hz in f_{rep}, corresponding to 310(10) kHz in absolute frequency. **c**, Bidirectional scan (Fig. 5, line b). To accelerate the experimental cycle in line centre determination for the four selected peaks, we use fast (400 s laser on and 200 s laser off) laser scan cycles. We perform scans by stepping f_{rep} in both positive and negative directions, and their results, after proper intensity normalization, are averaged to eliminate systematic shifts caused by potential line-shape asymmetries.

The comb frequencies are swept with a sawtooth profile over a 240 kHz scan range in the VUV. The starting frequency of the sawtooth is stepped by 240 kHz between cycles. During photon detection, the infrared beam is diverted from the cavity by an acousto-optic modulator. This completely turns off the VUV comb, removing any background from scattered light. We turn on the PMT to count individual fluorescent photons from the ^{229m}Th isomer decay for 200 s. The photon counts in each 1 s time bin are collected by using a digital counter.

Figure 2 shows the results of a full-range scan. In the middle panel, we plot the photon count rate averaged over the 200 s detection window as a function of f_{rep}. The background photon count rate of approximately 415 cps comes from the intrinsic radioactivity of the ^{229}Th:CaF_2 crystal[46]. On top of the background, six clear spectroscopic features are observed (highlighted in blue and green). In the bottom panel, we plot the count rate as a function of time after binning f_{rep} to approximately 15 mHz bins (approximately 400 kHz bin size in VUV frequency) to observe the time-dependent fluorescence for each scan step. We clearly see that the fluorescence from each feature persists beyond the 200 s detection window, consistent with the long lifetime[26] of ^{229m}Th embedded in CaF_2. We take the four strongest peaks (highlighted in green) from the scan to perform absolute frequency-determination measurements. The two weak peaks may originate from different electronic environments in the crystal and will be subject to future studies.

Line shape and centre frequency determination

To measure the lifetime of the ^{229m}Th state, we place one comb line on resonance and irradiate the crystal for 1,200 s. We then monitor the fluorescence count rate for approximately 90 min. The trace in Fig. 3a follows a clear exponential decay with a fitted time constant of $\tau = 641(4)$ s, consistent with the previously reported lifetime[26] of ^{229m}Th in CaF_2.

The long lifetime of the clock transition introduces a potential line shape asymmetry[26] when we measure with a 400 s laser on and 200 s laser off experiment cycle. Here, the excited-state population from one data point does not fully decay when we start the next measurement. To avoid this asymmetry, we first measure a fine line shape by using the same irradiation cycle, but wait 1,800 s, which is approximately three lifetimes, between adjacent frequency steps. This gives sufficient time for the ^{229m}Th to decay to the ground state. For each step here, we keep the excitation frequency fixed during irradiation. Figure 3b shows one such measurement by using this technique. A clear, symmetric line shape is observed and fit to a Gaussian.

To use the scanning time more efficiently, we perform bidirectional scans for subsequent measurements. Here, we use the same 400 s on and 200 s off experiment cycle but scan the line shape once by increasing f_{rep} and another time by decreasing f_{rep}. The scan range of each step is set to 100 kHz in the VUV. The two scans are each fit to Gaussian line shapes, and the line centre is determined by averaging the fit parameters from the two scans. Both line shapes have slight asymmetries owing to the short detection window, but the asymmetries cancel each other when the two scan directions are averaged. We obtain line centre uncertainties of approximately 4 kHz and full-width at half-maximum values of about 300 kHz. Figure 3c shows a forward, backward and averaged scan fit by using this method. The plotted frequency point corresponds to the centre frequency value of the scan range for each step. We use this bidirectional scan scheme for absolute frequency determination of the four peaks and for measuring the centre frequency of a fifth peak from electric quadrupole splitting (see below).

Comb mode determination

Although we illuminate the crystal with all the comb modes simultaneously, each spectroscopic feature corresponds to a nuclear excitation by one single comb mode. We use the technique previously demonstrated in ref. 37 to determine the comb mode number exciting the transition and convert the f_{rep} (radiofrequency) to the absolute frequency (VUV) of a given peak. We scan the same transition line with

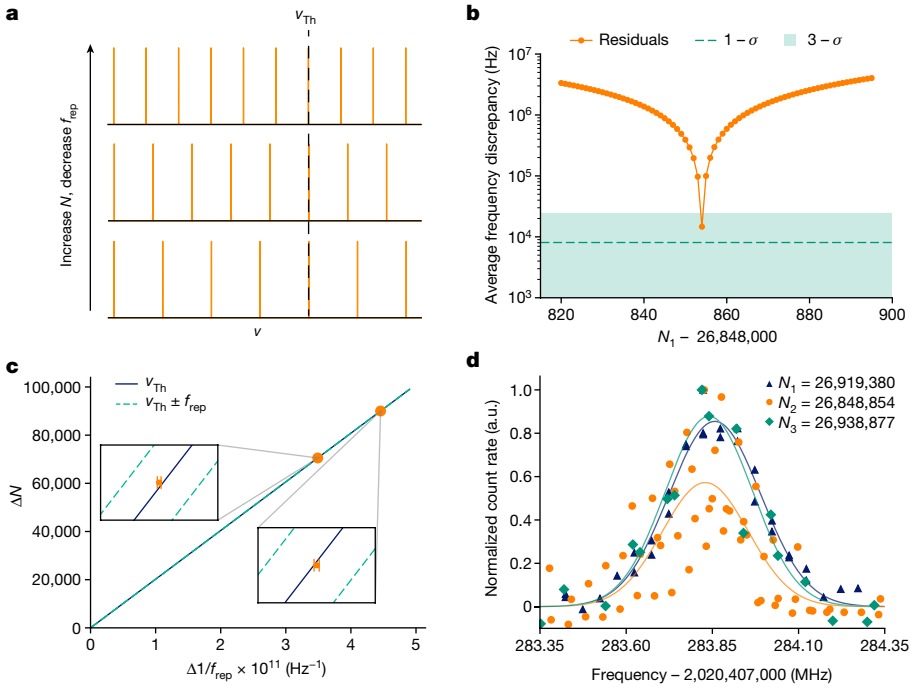

Fig. 4 | Absolute frequency determination. a, Illustration for absolute frequency determination. We precisely scan the same transition line by using three different values of f_{rep}. When these f_{rep} values are sufficiently different from each other and are yet precisely known, the exact mode number associated with each f_{rep} can be unambiguously determined[37]. **b**, Previous measurements[26,27] of the nuclear transition energy provides an initial guess range of about 80 possible comb mode numbers. Integer trial values of comb mode number N_1 in the first scan are picked and the transition frequencies are calculated accordingly. We force the comb mode number for the subsequent two measurements to the closest integer according to f_{rep} and calculate the transition frequency from them. The averaged frequency discrepancy between the measurements quantifies the comb mode assignment error. The lowest value of the discrepancy corresponds to the experimentally determined comb mode number assignment. The disagreement jumps by a factor of 10 when the comb mode is misassigned by ±1. The indicated $1-\sigma$ line and $3-\sigma$ region corresponds to the statistical uncertainty of the fitted Gaussian line centre. **c**, Another method for comb mode determination is to perform a linear fit between the mode number and the inverse value of f_{rep}. With an expanded view in the inset, we plot our measurement data for the two f_{rep} jumps, with the corresponding $1-\sigma$ error bars. The solid dark blue line corresponds to the comb mode number assignment N from **b**, in agreement with the measurement. Dashed green lines correspond to comb mode $N \pm 1$, in clear disagreement with our measurements. **d**, With the determination of the mode numbers, three scanned line shapes of a specific nuclear transition, corresponding to three different values of f_{rep} are plotted together against their absolute optical frequencies, confirming their consistency (a.u., arbitrary units).

three different comb mode numbers N_i (where i denotes the scan number) by shifting f_{rep}, as shown in Fig. 4a. These three distinct comb modes correspond to 100 kHz level jumps in f_{rep}. The jump step sizes are chosen such that they are much greater than the uncertainty in the fitted line centres in absolute frequency, which is approximately 4 kHz. In combination with the bounds on the transition frequency set by refs. 26,27, this allows us to determine the integer comb mode number exciting the line at each f_{rep} and thus the absolute frequency of the transition unambiguously. At each f_{rep} jump, we estimate the new f_{rep} position of each peak based on previous knowledge of the transition frequency and scan a small spectral region to find the exact position of the peak.

The uncertainty range of the nuclear transition at 2,020,408(3) GHz (given by the weighted average from refs. 26,27) corresponds to approximately 80 possible comb mode numbers $N_1 \approx 26{,}848{,}820$ to 26,848,900 for f_{rep_1}, shown on the x axis of Fig. 4b. These mode numbers are used to compute initial guesses for the absolute frequency ν_{Th}. Assuming this frequency ν_{Th} is correct, we use the fitted line centres at f_{rep_2} and f_{rep_3} to assign the closest integer comb mode N_2 and N_3. The comb equation can be written as:

$$\nu_{Th_i} = N_i f_{rep_i} + 7 f_{CEO}.$$

For the correct comb mode number assignment, the three ν_{Th} from f_{rep_1}, f_{rep_2} and f_{rep_3} should agree closely within uncertainty propagated from the fitted line centre. We quantify this as the average frequency discrepancy:

$$\frac{1}{3}\sum_{i=1}^{3} |\, \nu_{Th_i} - \nu_{Th_{avg}} \,|$$

where ν_{Th_i} is the transition frequency calculated from f_{rep_i} and N_i, and $\nu_{Th_{avg}}$ is the weighted average of the three ν_{Th}. As seen in Fig. 4b, the optimal comb mode assignment produces the lowest frequency discrepancy of 10 kHz, which is within the $3-\sigma$ region calculated from the uncertainty of the fitted line centre. A comb mode number assignment off by ±1 increases the average frequency discrepancy by an order of magnitude.

This optimal comb mode number assignment can also be visualized by using a linear fit based on a rearranged comb equation:

$$\Delta N = (\nu_{Th} - 7 f_{CEO})\,\Delta\frac{1}{f_{rep}}$$

where ΔN and $\Delta\frac{1}{f_{rep}}$ describe the change in comb mode number and inverse fitted peak centre from the highest repetition rate used, f_{rep_3}. The two points corresponding to the two lower values of f_{rep}, with error bars calculated from the uncertainties in the fitted line centres, are plotted in Fig. 4c. The insets provide an expanded view. The solid dark blue line passing through the origin with slope $\nu_{Th_{avg}} - 7 f_{CEO}$

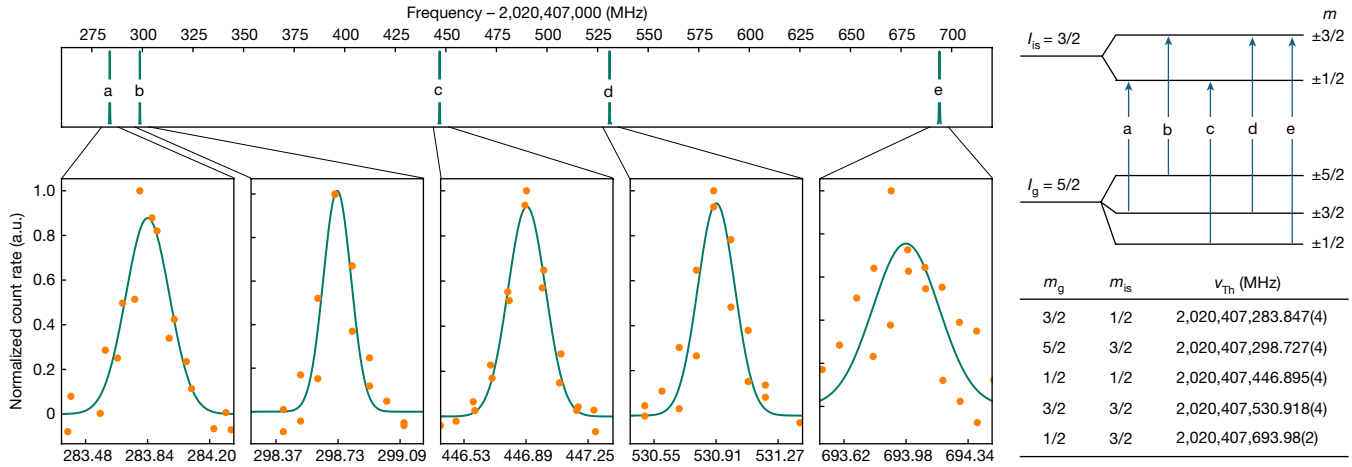

m_g	m_{is}	ν_{Th} (MHz)
3/2	1/2	2,020,407,283.847(4)
5/2	3/2	2,020,407,298.727(4)
1/2	1/2	2,020,407,446.895(4)
3/2	3/2	2,020,407,530.918(4)
1/2	3/2	2,020,407,693.98(2)

Fig. 5 | Direct spectroscopic measurement of nuclear electric quadrupole structure. The expected quadrupole line structure when ^{229}Th is subject to an electric field gradient inside the CaF_2 crystal (top right panel). With the absolute frequencies of lines a, b, c and d determined by the direct comb spectroscopy technique, their corresponding quantum numbers are uniquely assigned. An enlarged view shows the measurement data for each line, with their relative intensity normalized to unity. The frequency of line e, which is a factor of 10 weaker in line strength, was calculated first by using the relationship $\nu_e = \nu_c + \nu_d - \nu_a$, and then confirmed with a comb scan using a single comb mode. Absolute frequencies of the five transition lines are listed in the table.

corresponds to the optimal comb mode number assigned in Fig. 4b. The dashed green lines correspond to comb mode number assignments off by ±1, in clear disagreement with the measured data. The two analyses in Fig. 4b,c corroborate each other and demonstrate that we have assigned N_i with complete confidence.

With the comb mode numbers N_i for the three f_{rep} jumps uniquely determined for a given peak, we use the comb equation to convert from f_{rep} to absolute frequency. Figure 4d shows the three scans of the same peak (individually normalized) and their Gaussian fits plotted against absolute frequency, in which the legend displays the determined comb number. We see the three scans overlap, confirming the correct determination of the absolute frequency.

This procedure is repeated for the four chosen peaks in Fig. 2 (highlighted in green). The absolute frequency is then calculated as the weighted average between the three scans for each peak, which are tabulated in Fig. 5. The left panel shows the four peaks (labelled a–d) in absolute frequency, individually normalized with the data and fits from f_{rep_3} shown. The centre frequency of each line is determined to 4 kHz. The observed splittings are on the order of hundreds of megahertz, which is shown in the top panel.

Nuclear quadrupole structure

The four chosen lines are attributed to the nuclear electric quadrupole structure. As the ^{229}Th nuclei are embedded in a CaF_2 host, they experience a strong electric field gradient produced by the surrounding lattice ions and F^- interstitials[47]. The interaction between the electric quadrupole moment Q of the thorium nucleus and this electric field gradient gives rise to an electric quadrupole splitting, predicted to be on the order of hundreds of megahertz[29,30]. The splittings can be extracted from diagonalizing the Hamiltonian[47,48]:

$$H_{E2} = \frac{QV_{zz}}{4I(2I-1)}\left[3I_z^2 - \boldsymbol{I}^2 + \eta(I_x^2 - I_y^2)\right]$$

where Q is the spectroscopic nuclear electric quadrupole moment[17,25] in the ground (Q_g) or isomeric state (Q_{is}), and $\boldsymbol{I}$ is the nuclear angular momentum. The principal axis is chosen such that the electric field gradient matrix V_{ij} is diagonal and is thus described by its z component, V_{zz}, and an asymmetry parameter, $\eta = (V_{xx} - V_{yy})/V_{zz}$. The ground state of ^{229}Th has a nuclear spin $I_g = 5/2$, whereas the isomeric excited state has $I_{is} = 3/2$. Transitions with $\Delta m = 0, \pm 1$ are allowed by selection rules ($m = I_z$ is the z-axis angular momentum projection), although the asymmetry parameter η leads to state mixing and, therefore, additional weak transitions. However, they are not observed in this work and do not correspond to the two weak peaks highlighted in blue in Fig. 2. The upper right panel of Fig. 5 shows the level diagram with the four absolutely determined frequencies assigned to their corresponding sublevel transitions a–d.

Using the above equation, we fit the measured line centres to the predicted quadrupole structure using η, $Q_g V_{zz}$ and $Q_{is} V_{zz}$ as the fit parameters. This procedure yields $\eta = 0.59163(5)$, $Q_g V_{zz} = 339.258(7)$ eb V Å^{-2} and $Q_{is} V_{zz} = 193.387(5)$ eb V Å^{-2} (1 eb = 1.6022×10^{-47} C m^2 denotes one electron-barn). The extracted uncertainties are purely statistical. Independent of the crystal environment, the ratio of the quadrupole moments is extracted from the fitting procedure as $Q_{is}/Q_g = 0.57003(1)$, consistent with previously reported ratios[17,25] of 0.555(19) and 0.569(7). Taking the previously published[49] value of $Q_g = 3.11(2)$ eb, this yields an electric field gradient $V_{zz} = 109.1(7)$ V Å^{-2} for the CaF_2 crystal used in this experiment. In an upcoming publication, we will disentangle nuclear physics and material science by further exploring the quadrupole splittings as a function of material parameters.

In the initial full-range scan shown in Fig. 2, we did not observe the fifth line of the quadrupole structure, corresponding to the $m_g = \pm 1/2$ to $m_{is} = \pm 3/2$ transition (labelled 'e' on the diagram). From the Clebsch–Gordan coefficients, this line is predicted to have only one-tenth of the strength of the strongest line. Based on three of the known frequencies, we determine the expected absolute frequency of this fifth line by using the sum rule, $\nu_e = \nu_c + \nu_d - \nu_a = 2{,}020{,}407{,}693.966(7)$ MHz. We repeat the scan over the corresponding f_{rep} with our comb and indeed observe a weak line at 2,020,407,693.98(2) MHz. We determined this frequency with only a single f_{rep} step by using the expected comb mode number calculated from the expected line centre.

Thus, the five lines corresponding to the nuclear quadrupole structure of the ^{229m}Th transition have been measured and assigned, as shown in the table of Fig. 5. With proper averaging of the quadrupole splitting patterns (ignoring higher order moments), we can recover the unsplit transition frequency free of the electrical field gradient. The transition frequency between the $I = 5/2$ ground state and the $I = 3/2$ excited state is determined as:

$$\nu_{Th} = \frac{1}{6}(\nu_a + 2\nu_b + 2\nu_c + \nu_d) = 2{,}020{,}407{,}384{,}335(2)\,\text{kHz}.$$

Hence, we report the frequency ratio between the ^{229}Th nuclear clock transition and the ^{87}Sr atomic clock to be:

$$\frac{\nu_{\mathrm{Th}}}{\nu_{\mathrm{Sr}}} = 4.707072615078(5)$$

for ^{229}Th nuclei embedded in a CaF_2 host crystal at 150(1) K. The systematic uncertainty of this frequency ratio will be explored in future studies.

Discussion

Throughout the measurement campaign over two weeks, our measured line centres are consistent with each other within the measurement uncertainties, showing both the insensitivity of the ^{229}Th nuclear transition frequency to external environment changes and the precise absolute frequency control of our laser system referenced to the JILA ^{87}Sr clock[2]. The experimentally measured full-width at half-maximum of the nuclear resonance feature of around 300 kHz is most probably limited by the linewidth of our VUV frequency comb. During the cavity-enhanced harmonic generation process, the timing jitter of the fundamental laser is transferred to the upconverted light. Therefore, the seventh harmonic has a $7^2 = 49$ times higher phase noise power spectral density compared to that of the fundamental[38]. This can lead to a substantial broadening of the comb linewidth. Using a low-noise reference laser to stabilize the fundamental comb could drastically reduce the VUV comb linewidth to the hertz level[38], leading to orders of magnitude improved uncertainty of the transition line centre. This would allow us to probe the inhomogeneous broadening[29,30] in the host crystal, which is estimated to be a few hundred hertz.

Currently, the laser intensity (1 nW per comb mode focused to 0.2 mm diameter) and measured lifetime (641 s) correspond to a Rabi frequency of approximately 0.4 Hz, which is much smaller than the estimated inhomogeneous broadening[50]. Thus, to coherently control the nuclear state, a high-power VUV laser is needed. Now that the transition frequency has been precisely determined, a continuous wave laser with high output power can be built to address this transition. We note that efficient generation of VUV light in fibre systems[51] has also been demonstrated at kHz repetition rates, offering another possibility for scaling up the VUV comb power in a fibre-based system.

Although an optical clock can in principle operate based on detecting fluorescence photons from the clock transition[30], new approaches should be considered to accelerate the state detection. Akin to nuclear magnetic resonance, nuclear population in the ground and excited state manifold could be read out directly by using radiofrequency nuclear quadrupole resonance spectroscopy[8], reducing the time needed for clock operation and thus achieving better clock stability. X-ray quenching effects[12,24] provide another means to accelerate the readout scheme.

Systematic shifts and broadenings of the nuclear transition frequency, such as those due to crystal temperature and local magnetic field, will be characterized in our future studies. With the systematic shifts under control, we will establish a time record for the frequency ratio of $\nu_{\mathrm{Th}}/\nu_{\mathrm{Sr}}$. Given the significantly enhanced sensitivity of the nuclear clock to fundamental constants[11], we expect to provide improved bounds on the temporal variation of the fine-structure constant with moderately improved clock uncertainty.

To further improve the performance of a solid-state nuclear clock, important parameters of the crystal structure must be explored and understood. In particular, the origin of the two weak lines (Fig. 2, highlighted in light blue) in our full-range scan remains unknown and could be coming from ^{229}Th atoms doped in different charge compensation configurations within the crystal[47]. Studies comparing different host crystals[27], such as Th:$LiSrAlF_6$, could provide new insights. Differences in the electronic charge density and electric field gradient at the thorium nucleus in the $LiSrAlF_6$ crystal would lead to absolute frequency shifts and different splitting magnitude, respectively. These new measurements will provide important benchmarks for theoretical methods such as density functional theory[47] and will lead to new nuclear physics insights.

High-density quantum emitters with extremely long coherence times naturally provide a new system for quantum optics and quantum information studies. In our ^{229}Th:CaF_2 target, there are 10^4 atoms within a single λ^3 volume, where $\lambda \approx 148$ nm is the transition wavelength. In pure $^{229}ThF_4$ crystals, the number density can reach 10^{22} cm^{-3}, corresponding to 10^7 atoms inside a single λ^3 volume, providing opportunities to study collective effects and nuclear quantum optics when inhomogeneous effects in solids are brought under control. Suppressing dephasing and harnessing quantum resources[52] in solid-state ^{229}Th targets will directly benefit the development of a solid-state portable clock and create tremendous opportunities for quantum, laser and material science.

In conclusion, we have established a direct frequency link between the ^{229m}Th isomeric transition and the ^{87}Sr atomic clock. We have improved the precision of the ^{229}Th nuclear clock transition frequency by about six orders of magnitude and directly resolved the underlying nuclear quadrupole splitting. Our work provides a clear pathway forward to build and improve the nuclear clock. We herald the dawn of nuclear optical clocks that will enable numerous advances in fundamental physics, quantum physics and precision measurement technologies.

Online content

Any methods, additional references, Nature Portfolio reporting summaries, source data, extended data, supplementary information, acknowledgements, peer review information; details of author contributions and competing interests; and statements of data and code availability are available at https://doi.org/10.1038/s41586-024-07839-6.

1. Ludlow, A. D., Boyd, M. M., Ye, J., Peik, E. & Schmidt, P. O. Optical atomic clocks. *Rev. Mod. Phys.* **87**, 637–701 (2015).
2. Aeppli, A., Kim, K., Warfield, W., Safronova, M. S. & Ye, J. Clock with 8×10^{-19} systematic uncertainty. *Phys. Rev. Lett.* **133**, 023401 (2024).
3. Peik, E. & Tamm, C. Nuclear laser spectroscopy of the 3.5 eV transition in Th-229. *EPL – Europhys. Lett.* **61**, 181 (2003).
4. Tkalya, E. V., Varlamov, V. O., Lomonosov, V. V. & Nikulin, S. A. Processes of the nuclear isomer ^{229m}Th(3/2$^+$, 3.5 ± 1.0 eV) resonant excitation by optical photons. *Phys. Scr.* **53**, 296 (1996).
5. Bothwell, T. et al. Resolving the gravitational redshift across a millimetre-scale atomic sample. *Nature* **602**, 420–424 (2022).
6. Ye, J. & Zoller, P. Essay: quantum sensing with atomic, molecular, and optical platforms for fundamental physics. *Phys. Rev. Lett.* **132**, 190001 (2024).
7. von der Wense, L. & Seiferle, B. The ^{229}Th isomer: prospects for a nuclear optical clock. *Eur. Phys. J. A* **56**, 277 (2020).
8. Peik, E. et al. Nuclear clocks for testing fundamental physics. *Quantum Sci. Technol.* **6**, 034002 (2021).
9. Beeks, K. et al. The thorium-229 low-energy isomer and the nuclear clock. *Nat. Rev. Phys.* **3**, 238–248 (2021).
10. Flambaum, V. V. Enhanced effect of temporal variation of the fine structure constant and the strong interaction in ^{229}Th. *Phys. Rev. Lett.* **97**, 092502 (2006).
11. Fadeev, P., Berengut, J. C. & Flambaum, V. V. Sensitivity of ^{229}Th nuclear clock transition to variation of the fine-structure constant. *Phys. Rev. A* **102**, 052833 (2020).
12. Nickerson, B. S. et al. Driven electronic bridge processes via defect states in ^{229}Th-doped crystals. *Phys. Rev. A* **103**, 053120 (2021).
13. Helmer, R. G. & Reich, C. W. An excited state of ^{229}Th at 3.5 eV. *Phys. Rev. C* **49**, 1845–1858 (1994).
14. Guimarães-Filho, Z. O. & Helene, O. Energy of the 3/2$^+$ state of ^{229}Th reexamined. *Phys. Rev. C* **71**, 044303 (2005).
15. Beck, B. R. et al. Energy splitting of the ground-state doublet in the nucleus ^{229}Th. *Phys. Rev. Lett.* **98**, 142501 (2007).
16. Beck, B. R. et al. *Improved Value for the Energy Splitting of the Ground-State Doublet in the Nucleus ^{229m}Th* Report No. LLNL-PROC-415170 (Lawrence Livermore National Laboratory, 2009).
17. Thielking, J. et al. Laser spectroscopic characterization of the nuclear-clock isomer ^{229m}Th. *Nature* **556**, 321–325 (2018).
18. Seiferle, B. et al. Energy of the ^{229}Th nuclear clock transition. *Nature* **573**, 243–246 (2019).
19. Masuda, T. et al. X-ray pumping of the ^{229}Th nuclear clock isomer. *Nature* **573**, 238–242 (2019).
20. Yamaguchi, A. et al. Energy of the ^{229}Th nuclear clock isomer determined by absolute γ-ray energy difference. *Phys. Rev. Lett.* **123**, 222501 (2019).
21. Sikorsky, T. et al. Measurement of the ^{229}Th isomer energy with a magnetic microcalorimeter. *Phys. Rev. Lett.* **125**, 142503 (2020).

22. von der Wense, L. et al. Direct detection of the ^{229}Th nuclear clock transition. *Nature* **533**, 47–51 (2016).
23. Kraemer, S. et al. Observation of the radiative decay of the ^{229}Th nuclear clock isomer. *Nature* **617**, 706–710 (2023).
24. Hiraki, T. et al. Controlling ^{229}Th isomeric state population in a VUV transparent crystal. *Nat. Commun.* **15**, 5536 (2024).
25. Yamaguchi, A. et al. Laser spectroscopy of triply charged ^{229}Th isomer for a nuclear clock. *Nature* **629**, 62–66 (2024).
26. Tiedau, J. et al. Laser excitation of the Th-229 nucleus. *Phys. Rev. Lett.* **132**, 182501 (2024).
27. Elwell, R. et al. Laser excitation of the ^{229}Th nuclear isomeric transition in a solid-state host. *Phys. Rev. Lett.* **133**, 013201 (2024).
28. Tkalya, E. V. Spontaneous emission probability for M1 transition in a dielectric medium: ^{229m}Th ($3/2^+$, 3.5±1.0 eV) decay. *JETP Lett.* **71**, 311–313 (2000).
29. Rellergert, W. G. et al. Constraining the evolution of the fundamental constants with a solid-state optical frequency reference based on the ^{229}Th nucleus. *Phys. Rev. Lett.* **104**, 200802 (2010).
30. Kazakov, G. A. et al. Performance of a ^{229}Thorium solid-state nuclear clock. *New J. Phys.* **14**, 083019 (2012).
31. Oelker, E. et al. Demonstration of 4.8×10^{-17} stability at 1 s for two independent optical clocks. *Nat. Photon.* **13**, 714–719 (2019).
32. Milner, W. R. et al. Demonstration of a timescale based on a stable optical carrier. *Phys. Rev. Lett.* **123**, 173201 (2019).
33. Diddams, S. A., Vahala, K. & Udem, T. Optical frequency combs: coherently uniting the electromagnetic spectrum. *Science* **369**, eaay3676 (2020).
34. Dreissen, L. S. et al. High-precision Ramsey-comb spectroscopy based on high-harmonic generation. *Phys. Rev. Lett.* **123**, 143001 (2019).
35. Jones, R. J., Moll, K. D., Thorpe, M. J. & Ye, J. Phase-coherent frequency combs in the vacuum ultraviolet via high-harmonic generation inside a femtosecond enhancement avity. *Phys. Rev. Lett.* **94**, 193201 (2005).
36. Gohle, C. et al. A frequency comb in the extreme ultraviolet. *Nature* **436**, 234–237 (2005).
37. Cingöz, A. et al. Direct frequency comb spectroscopy in the extreme ultraviolet. *Nature* **482**, 68–71 (2012).
38. Benko, C. et al. Extreme ultraviolet radiation with coherence time greater than 1 s. *Nat. Photon.* **8**, 530–536 (2014).
39. Pupeza, I., Zhang, C., Högner, M. & Ye, J. Extreme-ultraviolet frequency combs for precision metrology and attosecond science. *Nat. Photon.* **15**, 175–186 (2021).
40. Zhang, C. et al. Tunable VUV frequency comb for ^{229m}Th nuclear spectroscopy. *Opt. Lett.* **47**, 5591 (2022).
41. Ycomb - Compact frequency comb. *IMRA* https://www.imra.com/products/imra-scientific/ycomb-100 (2021).
42. Pronin, O. et al. Ultrabroadband efficient intracavity XUV output coupler. *Opt. Express* **19**, 10232–10240 (2011).
43. Fischer, J. et al. Efficient XUV-light out-coupling of intra-cavity high harmonics by a coated grazing-incidence plate. *Opt. Express* **30**, 30969–30979 (2022).
44. Beeks, K. et al. Growth and characterization of thorium-doped calcium fluoride single crystals. *Sci. Rep.* **13**, 3897 (2023).
45. Beeks, K. et al. Optical transmission enhancement of ionic crystals via superionic fluoride transfer: growing VUV-transparent radioactive crystals. *Phys. Rev. B* **109**, 094111 (2024).
46. Stellmer, S., Schreitl, M. & Schumm, T. Radioluminescence and photoluminescence of Th:CaF_2 crystals. *Sci. Rep.* **5**, 15580 (2015).
47. Dessovic, P. et al. ^{229}Thorium-doped calcium fluoride for nuclear laser spectroscopy. *J. Phys. Condens. Matter* **26**, 105402 (2014).
48. Dunlap, B. D. & Kalvius, G. M. in *Handbook on the Physics and Chemistry of the Actinides* Vol. 2 (eds Freeman, A. J. & Lander, G. H.) 331–434 (Elsevier Science, 1985).
49. Porsev, S. G., Safronova, M. S. & Kozlov, M. G. Precision calculation of hyperfine constants for extracting nuclear moments of ^{229}Th. *Phys. Rev. Lett.* **127**, 253001 (2021).
50. von der Wense, L. & Zhang, C. Concepts for direct frequency-comb spectroscopy of ^{229m}Th and an internal-conversion-based solid-state nuclear clock. *Eur. Phys. J. D* **74**, 146 (2020).
51. Travers, J. C., Grigorova, T. F., Brahms, C. & Belli, F. High-energy pulse self-compression and ultraviolet generation through soliton dynamics in hollow capillary fibres. *Nat. Photon.* **13**, 547–554 (2019).
52. Liao, W.-T., Das, S., Keitel, C. H. & Pálffy, A. Coherence-enhanced optical determination of the ^{229}Th isomeric transition. *Phys. Rev. Lett.* **109**, 262502 (2012).
53. Jain, A. et al. Commentary: The Materials Project: A materials genome approach to accelerating materials innovation. *APL Mater.* **1**, 011002 (2013).

Methods

Frequency locking and scan parameters

We fully stabilize the frequency comb by locking it at two spectral points. First, we lock a specific comb mode to the ^{87}Sr atomic clock. Second, we lock the carrier-envelope offset frequency f_{CEO} to a radiofrequency reference. The comb scan is accomplished by changing the offset frequency between one comb mode and the stable Sr clock laser (Extended Data Fig. 1). In brief, supercontinuum light is generated in the preamplified comb via a highly nonlinear photonic crystal fibre. Part of the supercontinuum light is also doubled by using a periodically poled lithium niobate crystal. These two beams are beat against one another for the f_{CEO} detection using the f–$2f$ scheme in an all-fibre setup[54]. We stabilize the f_{CEO} by feeding back to the oscillator pump current. The lock gain sign and reference frequency are chosen such that we effectively stabilize the frequency of a virtual comb line corresponding to the comb f_{CEO} to −8 MHz.

The supercontinuum comb light is also beat against the Sr clock laser at 698 nm to generate f_{beat}. We use the error signal from f_{beat} to slowly steer the frequency of a narrow linewidth Mephisto laser centred at 1,064 nm. The Mephisto laser is beat against the fundamental comb light. We stabilize the comb-Mehpisto beatnote by applying fast feedback to the comb oscillator cavity length by using a piezo actuator along with an intraoscillator electro-optical modulator. Scans are achieved by sweeping the f_{beat} lock point with a direct digital synthesizer. Directly locking our comb to a narrow linewidth Mephisto laser near the fundamental spectrum reduces the comb phase noise and narrows the comb linewidth. The Mephisto laser is additionally coupled to the femtosecond enhancement cavity and is used to stabilize the cavity length by using the Pound–Drever–Hall locking scheme[55]. An acousto-optic modulator is used to add an offset frequency to the Mephisto, allowing us to change the detuning between the frequency comb and cavity resonance. This comb–cavity detuning is used to mitigate cavity bistability caused by intracavity plasma nonlinearities[56,57].

Crystal growth and properties

A thorium-doped calcium fluoride (Th:CaF_2) crystal was grown at TU Wien and cut (named 'tiny-X2') from the ingot with the highest ^{229}Th doping concentration (5×10^{18}cm^{-3}) so far. This ingot, 'X2' (3.2 mm diameter, 10 mm long cylinder), is used in both the first laser excitation of the ^{229}Th nucleus at PTB[26] and the ^{229}Th population control at Spring-8 (ref. 24). Owing to the radioactivity of ^{229}Th, the crystal luminesces in the VUV and UV through Cherenkov radiation and annihilation of self-trapped-excitons, respectively[58]. Therefore, it is beneficial to match the crystal size to the excitation source spot size (0.2 mm) to maximize the signal and reduce VUV and UV background. A corner of a X2 cylinder is cut (for methods, see ref. 58) by using a 0.08 mm diamond wire saw such that the surface facing the laser has two edges at 90° degrees: 0.7 mm in width and 1.8 mm in height. The third edge of this surface is an arc with a radius of 1.6 mm. The depth of the crystal is 1.4 mm.

The original ingot X2 was grown under vacuum by using a miniaturized version of the vertical gradient freeze method with single crystalline CaF_2 as the seed. As described in detail in ref. 44, the ^{229}Th doping material is inserted in a pocket in the seed crystal before growth by preparing a $^{229}ThF_4$:PbF_2:CaF_2 precipitate as a carrier to facilitate physical handling of the less than 1 mg of ^{229}Th. In the vertical gradient freeze procedure, the top part of the seed melts, and subsequently a single crystalline Th:CaF_2 is grown as the melt is slowly cooled. The PbF_2 acts as an oxygen scavenger and evaporates. During growth, the radioactivity of ^{229}Th induces radiolysis in the melt, which causes evaporation of F_2, resulting in a fluoride-deficient non-stoichiometric Th:CaF_2 crystal. The fluoride deficiency causes formation of Ca metallic inclusions, which through Mie scattering[59] cause a reduction of the crystal transparency at the isomer wavelength. By using superionic fluoride transfer, as described in ref. 45, fluoride is added to the crystal efficiently without losing the single-crystal structure, recovering the VUV transparency. The crystal properties of tiny-X2 are shown in Extended Data Table 1.

Spectroscopy system alignment

The thorium-doped CaF_2 crystal is glued onto a MgF_2 plate and mounted inside the vacuum chamber. A liquid nitrogen dewar is installed to the top of the chamber, which is connected to the crystal mount via a cold finger and copper thermal link. The link is attached in a configuration that would minimize fluorescent photon loss. A temperature sensor attached to the mount monitors the crystal temperature during scan operation. The operating temperature remains stable at approximately 150(1) K during all scans.

Figure 1c shows the proper alignment of the VUV comb to the crystal. The blue fluorescence from the crystal serves as a monitor of the VUV power and an alignment check. When the beam is aligned correctly, a blue fluorescent line can be seen passing through the entire crystal. The VUV beam is terminated at a Ce:YAG scintillation plate for alignment and power monitoring, and to avoid damage of the PMT downstream in the optical beam path.

The crystal is placed at the focal point of the VUV-reflective parabolic mirror. The mirror has a 12 mm diameter hole in the vertex to allow the VUV beam to pass through. Fluorescent photons from the crystal are collimated by the parabolic mirror with a geometrical collection efficiency[60] of approximately 0.4. The photons are spectrally filtered by three dichroic mirrors and focused via a MgF_2 lens to the PMT.

Data availability

The data that support the findings of this study are available from the corresponding author upon appropriate request.

54. Sinclair, L. C. et al. Invited article: a compact optically coherent fiber frequency comb. *Rev. Sci. Instrum.* **86**, 081301 (2015).
55. Black, E. D. An introduction to Pound–Drever–Hall laser frequency stabilization. *Am. J. Phys.* **69**, 79–87 (2001).
56. Allison, T. K., Cingöz, A., Yost, D. C. & Ye, J. Extreme nonlinear optics in a femtosecond enhancement cavity. *Phys. Rev. Lett.* **107**, 183903 (2011).
57. Yost, D. C. et al. Power optimization of XUV frequency combs for spectroscopy applications [Invited]. *Opt. Express* **19**, 23483–23493 (2011).
58. Beeks, K. The nuclear excitation of thorium-229 in the CaF_2 environment: development of a crystalline nuclear clock. PhD thesis, Technische Universität, Wien (2022).
59. Rix, S. et al. Formation of metallic colloids in CaF_2 by intense ultraviolet light. *Appl. Phys. Lett.* **99**, 261909–261909 (2011).
60. Seiferle, B., von der Wense, L., Laatiaoui, M. & Thirolf, P. G. A VUV detection system for the direct photonic identification of the first excited isomeric state of ^{229}Th. *Eur. Phys. J. D* **70**, 58 (2016).

Acknowledgements We thank K. Kim, A. Aeppli, W. Warfield and W. Milner for building and maintaining the JILA ^{87}Sr optical clock; D. Lee, Z. Hu and B. Lewis for building and maintaining the JILA stable laser and the cryogenic Si cavity; the entire crystal growth team at TU Wien for preparation of the thorium-doped crystal; M. E. Fermann and J. Jiang for help in constructing the high-power infrared frequency comb; K. Hagen, C. Schwadron, K. Thatcher, H. Green, D. Warren and J. Uhrich for help in designing and building mechanical parts used in the detection setup; T. Brown and I. Ryger for help in designing and making electronics used in the experiment; M. Ashton, B. C. Denton and M. R. Statham for help in the shipment of radioactive samples; E. Hudson, E. Peik, J. Hur, J. Thompson, J. Weitenberg and A. Ozawa for helpful discussions; and IMRA America for collaboration. We acknowledge funding support from the Army Research Office (grant no. W911NF2010182), the Air Force Office of Scientific Research (grant no. FA9550-19-1-0148), the National Science Foundation (grant no. QLCI OMA-2016244), the National Science Foundation (grant no. PHY-2317149) and the National Institute of Standards and Technology. J.S.H. acknowledges support from a National Research Council Postdoctoral Fellowship. L.v.d.W. acknowledges funding from a Feodor Lynen fellowship from the Humboldt Foundation. P.G.T. acknowledges support from the European Research Council (Horizon 2020, grant no. 856415) and the European Union's Horizon 2020 Programme (grant no. 664732). The ^{229}Th:CaF_2 crystal was grown in TU Wien with support from the European Research Council (Horizon 2020, grant no. 856415) and the Austrian Science Fund (grant DOI: 10.55776/F1004, 10.55776/J4834 and 10.55776/ PIN9526523). The project 23FUN03 HIOC (grant DOI: 10.13039/100019599) has received funding from the European Partnership on Metrology, co-financed from the European Union's Horizon Europe Research and Innovation Programme and by the participating states. We thank the National Isotope Development Center of DoE and Oak Ridge National Laboratory for providing the Th-229 used in this work.

Author contributions C.Z., T.O., J.S.H., J.F.D., L.v.d.W., K.B., T.S. and J.Y. conceived and planned the experiment; K.B., A.L., G.A.K. and T.S. grew the thorium-doped crystal and characterized its performance; P.G.T. provided valuable insight and the parabolic mirror; and C.Z., T.O., J.S.H., J.F.D., L.v.d.W., P.L. and J.Y. performed the measurement and analysed the data. All authors wrote the manuscript.

Competing interests The authors declare no competing interests.

Additional information

Supplementary information The online version contains supplementary material available at https://doi.org/10.1038/s41586-024-07839-6.

Correspondence and requests for materials should be addressed to Chuankun Zhang or Jun Ye.

Peer review information *Nature* thanks Nicola Poli and the other, anonymous, reviewer(s) for their contribution to the peer review of this work. Peer reviewer reports are available.

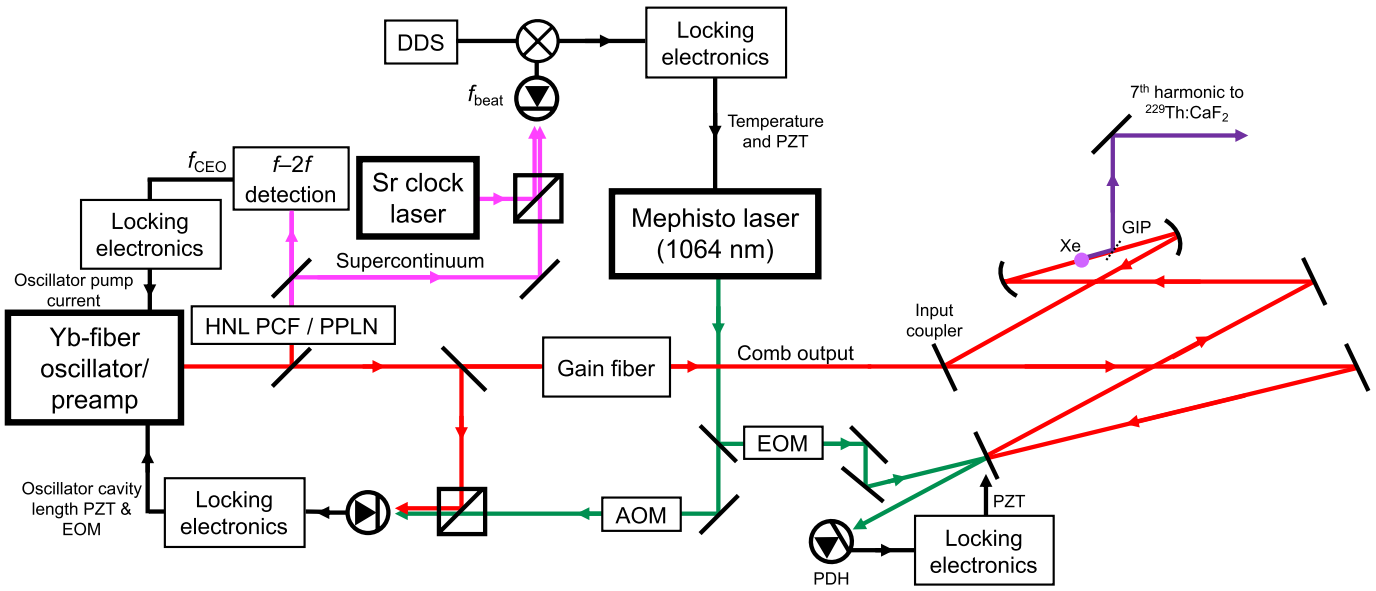

Extended Data Fig. 1 | Locking scheme used in our experimental setup. A Yb-fiber oscillator is used to generate the fundamental frequency comb[40]. The light is amplified using a chirped pulse amplification scheme in a large mode area gain fiber. The output comb light (average power 40–50 W) is coupled to a femtosecond enhancement cavity with finesse ~600 to further enhance the peak power for efficient cavity-enhanced high harmonic generation. The 7th harmonic is outcoupled using a grazing incidence plate[42,43] (GIP) and directed to the sample chamber. A portion of the pre-amplified comb light is picked off and focused to a highly nonlinear photonic crystal fiber (HNL PCF) for broadband supercontinuum generation. The light is also doubled using a periodically poled lithium niobate (PPLN) crystal. These two beams generate a beatnote that directly reports on f_{CEO} (*f–2f* detection), which can be fed back to the pump current for f_{CEO} locking. The supercontinuum light is beatnote locked against the Sr clock light at 698 nm through an auxiliary narrow linewidth Mephisto laser at 1064 nm. The beatnote f_{beat} is mixed with a DDS output and is used to steer the Mephisto laser frequency. The Mephisto output is passed through a fiber acousto-optic modulator (AOM) to generate a frequency offset and is beat against a portion of the preamplified fundamental comb light. The control signal is fed back to the oscillator cavity length to close the loop for the f_{beat} lock. We conduct our scans by changing the DDS offset frequency, which ultimately changes the comb repetition frequency without shifting f_{CEO}. An additional portion of the Mephisto light is picked off and modulated with an electro-optical modulator (EOM) for Pound-Drever-Hall locking of the enhancement cavity. The offset between the locked cavity resonance and the fundamental frequency comb can be tuned by adjusting the AOM offset frequency to mitigate intracavity plasma instabilities[56,57]. PZT, piezo-electric actuator.

Extended Data Table 1 | Properties of Tiny-X2 crystal

Base area	0.823 mm^2
Weight	3.7 mg
Column density	8×10^{15} mm^{-1}
Activity	18.1 kBq
Transmission	45% at 150 nm

Physical dimensions and properties of the Tiny-X2 crystal are listed in the table.

Terms and Conditions

Springer Nature journal content, brought to you courtesy of Springer Nature Customer Service Center GmbH (“Springer Nature”).
Springer Nature supports a reasonable amount of sharing of research papers by authors, subscribers and authorised users (“Users”), for small-scale personal, non-commercial use provided that all copyright, trade and service marks and other proprietary notices are maintained. By accessing, sharing, receiving or otherwise using the Springer Nature journal content you agree to these terms of use (“Terms”). For these purposes, Springer Nature considers academic use (by researchers and students) to be non-commercial.
These Terms are supplementary and will apply in addition to any applicable website terms and conditions, a relevant site licence or a personal subscription. These Terms will prevail over any conflict or ambiguity with regards to the relevant terms, a site licence or a personal subscription (to the extent of the conflict or ambiguity only). For Creative Commons-licensed articles, the terms of the Creative Commons license used will apply.
We collect and use personal data to provide access to the Springer Nature journal content. We may also use these personal data internally within ResearchGate and Springer Nature and as agreed share it, in an anonymised way, for purposes of tracking, analysis and reporting. We will not otherwise disclose your personal data outside the ResearchGate or the Springer Nature group of companies unless we have your permission as detailed in the Privacy Policy.
While Users may use the Springer Nature journal content for small scale, personal non-commercial use, it is important to note that Users may not:

1. use such content for the purpose of providing other users with access on a regular or large scale basis or as a means to circumvent access control;
2. use such content where to do so would be considered a criminal or statutory offence in any jurisdiction, or gives rise to civil liability, or is otherwise unlawful;
3. falsely or misleadingly imply or suggest endorsement, approval , sponsorship, or association unless explicitly agreed to by Springer Nature in writing;
4. use bots or other automated methods to access the content or redirect messages
5. override any security feature or exclusionary protocol; or
6. share the content in order to create substitute for Springer Nature products or services or a systematic database of Springer Nature journal content.

In line with the restriction against commercial use, Springer Nature does not permit the creation of a product or service that creates revenue, royalties, rent or income from our content or its inclusion as part of a paid for service or for other commercial gain. Springer Nature journal content cannot be used for inter-library loans and librarians may not upload Springer Nature journal content on a large scale into their, or any other, institutional repository.
These terms of use are reviewed regularly and may be amended at any time. Springer Nature is not obligated to publish any information or content on this website and may remove it or features or functionality at our sole discretion, at any time with or without notice. Springer Nature may revoke this licence to you at any time and remove access to any copies of the Springer Nature journal content which have been saved.
To the fullest extent permitted by law, Springer Nature makes no warranties, representations or guarantees to Users, either express or implied with respect to the Springer nature journal content and all parties disclaim and waive any implied warranties or warranties imposed by law, including merchantability or fitness for any particular purpose.
Please note that these rights do not automatically extend to content, data or other material published by Springer Nature that may be licensed from third parties.
If you would like to use or distribute our Springer Nature journal content to a wider audience or on a regular basis or in any other manner not expressly permitted by these Terms, please contact Springer Nature at

onlineservice@springernature.com